# Quantum particle localization by frequent coherent monitoring

Goren Gordon,[1] Igor E. Mazets,[2,3] and Gershon Kurizki[1]
[1]*Department of Chemical Physics, Weizmann Institute of Science, Rehovot 76100, Israel*
[2]*Vienna Center for Quantum Science and Technology, Atominstitut, TU Wien, 1020 Vienna, Austria*
[3]*Ioffe Physico-Technical Institute of the Russian Academy of Sciences, 194021 St. Petersburg, Russia*
(Received 22 February 2013; revised manuscript received 10 May 2013; published 31 May 2013)

We present an approach to monitoring and controlling a free quantum particle by coupling an internal (discrete) state of the particle to a detector (or probe). We consider a sequence of time-dependent, spatially localized interactions of the particle with the probe that are *purely coherent* (nondissipative), without mean energy-momentum exchange. We show that a sequence of such force-free interactions can freeze or deflect the particle.

DOI: 10.1103/PhysRevA.87.052141 PACS number(s): 03.65.Xp, 03.65.Ta, 03.65.Yz

## I. INTRODUCTION

Schrödinger argued that quantum mechanics, particularly the wave-particle duality, can be inferred from one principle: the impossibility of continuous observation [1]. Yet this principle has not been exhaustively scrutizined thus far. Studies of position measurements of freely propagating quantum particles [2–4] typically assume *continuous* (*static*) interaction with a spatially inhomogeneous probe (detector) regarded as a bath. The common denominator of such studies is that the particle's wave packet is localized by a spatially inhomogeneous complex potential (and therefore a force) associated with a bath [2–6].

We here put forward an alternative approach to monitoring a wave packet that describes a free quantum particle. This approach is realizable by coupling an internal (discrete) state of the particle to a detector (probe), such that the probe-induced transition from that state to another state signals the presence of the particle (Fig. 1). Unlike previous models [2–8], we consider a sequence of time-dependent, spatially localized interactions of the particle with the probe that to a good approximation are *purely coherent* (nondissipative), so that no coupling to a bath is invoked. These interactions may be designed to be "elastic," without mean energy-momentum exchange so that allegedly no force is involved. Yet, because the interactions are with probe beams of *finite width*, momentum (force) uncertainty is necessarily incurred by the process. We show that a sequence of such "force-free" interactions, here denoted as "premeasurements" (PMs) can freeze or deflect the particle. Due to orthogonality between the wave packets corresponding to different internal states, our PM monitoring consists in repeated interferences within each of the orthogonal wave packets.

The predicted effects are essentially different from the quantum Zeno effect [9] or its inverse (the anti-Zeno effect) [10–14], i.e., the respective slowdown or speedup of quantum-state change by frequent observations. Although such effects have mostly been studied for discrete variables [7–9,13,15–19], frequent observations of position have also been considered [8] under the idealized assumption of projective measurements that fully localize the particles (which would create nearly infinite effective potential barriers). We here adopt an experimentally feasible model of frequent PM monitoring that may appear to be the quantum analog of the Zeno arrow paradox, whereby a frequently watched arrow does not fly. Yet, remarkably, excessively frequent PMs are shown to hamper localization, which requires specific timings, contrary to either Zeno-like or anti-Zeno evolution [7–19]. Hence, we are dealing with an essentially different monitoring regime.

## II. MODEL AND PROCEDURE

We consider a free particle that interacts with a probe, with states $|0\rangle$ and $|1\rangle$. The probe may be a detecting light beam or internal states of the particle itself, e.g., energy states of an atom or polarization states of a photon. We require the mean energy and momentum of the particle not to change by a transition between the internal states of the probe, so that no classical force is exerted by the transition.

The total Hamiltonian of the particle ($S$) and probe ($P$) is given by

$$H(t,x) = H_S \otimes I_P + I_S \otimes H_P + H_{SP}(t,x), \tag{1}$$

$$H_{SP}(t,x) = V(t,x)\sigma_x, \tag{2}$$

where $H_S$ is the system (free-particle) Hamiltonian, $\sigma_x = |1\rangle\langle 0| + |0\rangle\langle 1|$, and $V(t,x)$ is the system-probe (detector) interaction operator. For our plots, we choose $H_P = 0$, reflecting energy degeneracy of the probe states $|0\rangle$ and $|1\rangle$, to simplify the analysis and accentuate its nonclassical aspects [Figs. 1(a)]. The system-probe interaction is taken to have the spatiotemporal form $V(t,\boldsymbol{x}) = \hbar g u(\boldsymbol{x}) f(t)$, where $g$, $u(\boldsymbol{x})$, and $f(t)$ are the coupling strength and spatial and temporal profiles, respectively. Specifically we shall take $f(t) = \frac{\sqrt{\pi}}{2T}\sum_n e^{-(t-n\tau)^2/T^2}$ to be a sequence of $n$ temporally Gaussian interactions of mean duration $T$ and separation $\tau$.

The static or continuous limit of time-independent $V(\mathbf{x}) = \pi\hbar g u(\mathbf{x})/(2\tau)$ is obtained upon taking $T \gg \tau$, while the dynamic impulsive limit is that of $T \ll \tau$. The coupling is chosen to achieve complete transfer from $|0\rangle$ to $|1\rangle$ after each period of the system-probe interaction sequence at the spatial profile peak $u(0) = 1$. In other words, we choose the coupling strength $g$ such that $g\int_0^\tau dt\, f(t) = \pi/2$ in the impulsive limit and $g = 1$ in the static or continuous limit.

The particle wave function is subject to the translational-internal entanglement (TIE) [20,21] induced by the probe. It is given by

$$|\psi(t,\boldsymbol{x})\rangle = \psi_0(t,\boldsymbol{x})|0\rangle + \psi_1(t,\boldsymbol{x})|1\rangle. \tag{3}$$

 ©2013 American Physical Society

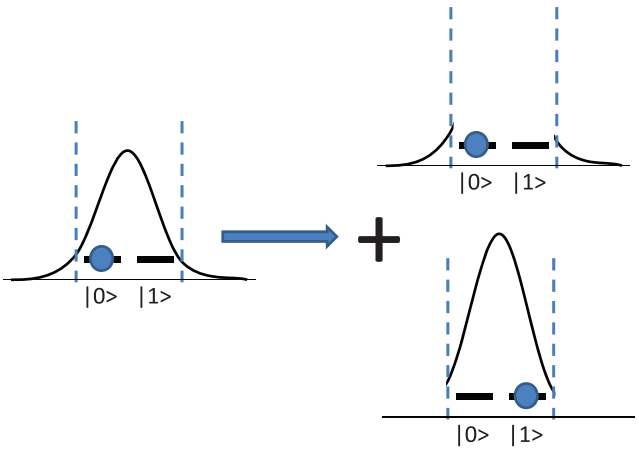


FIG. 1. (Color online) Schematic diagram of localization process: an initial Gaussian wave packet with two degenerate internal degrees of freedom (probe) undergoes translational-internal entanglement (TIE) due to a localized (vertical dashed lines) interaction.

We can allow for the effect of decoherence ("proper dephasing") of the $|1\rangle \leftrightarrow |0\rangle$ transition at a rate $R$, concurrent with the system-probe interaction, which results in degradation of the induced system-probe entanglement [22] and changes the wave function into a mixed state (see below). The limit of strong decoherence corresponds to uncorrelated interactions separated by the interval $\tau$, which amounts to using a new probe at each interaction. Yet it is the opposite limit of weak (or negligible) decoherence $R \ll 1/\tau$, corresponding to *correlated* acts of TIE, that is shown to cause the most spectacular effects.

Two procedures will be compared: (i) Repeated selective measurements (SMs), wherein the probe is read at times $t = n\tau$, $n = 1, \ldots, N$, thus collapsing the wave packet to the appropriate form after each interaction: if $|0\rangle(|1\rangle)$ is measured, $\psi(n\tau, \boldsymbol{x}) = \psi_{0(1)}(n\tau, \boldsymbol{x})/\sqrt{P_{0(1)}(n\tau)}$, where $P_{0(1)}(n\tau) = \int_{-\infty}^{\infty} d\boldsymbol{x} |\psi_{0(1)}(n\tau, \boldsymbol{x})|^2$ is the probability of that measurement result. (ii) Premeasurements, whereby *no action is taken*, apart from repeated TIEs. As argued below, the latter procedure amounts to tracing out the internal (probe) states, resulting in a statistical mixture of the two wave packets, each undergoing separate correlated interferences.

## III. RESULTS

We wish to compare the wave-packet dynamics caused by SMs and PMs, respectively, in both continuous static and impulsive (dynamic) monitoring regimes. Two major effects transpire from their numerical study:

(a) *Localization* ("freezing") (Fig. 2). We find the possibility of strong trapping or freezing a particle by frequently monitoring it at its initial location, via a spatially localized probe. Localization is here characterized by the probability of the particle being within the detector's profile $u(\boldsymbol{x})$ at time $t$ (Fig. 1): in one dimension (1D) $p(t) = \int_{-\infty}^{\infty} dx u(x) \langle x|\rho_+(t,x)|x\rangle$, where $\langle x|\rho_+(t)|x\rangle = \langle x|[\rho_{00}(t,x) + \rho_{11}(t,x)]|x\rangle$ is the probability density under PM (the sum of $|0\rangle$ and $|1\rangle$ probabilities), Fig. 3. PMs are shown to cause much more effective localization than SMs, and impulsive monitoring is more effective than

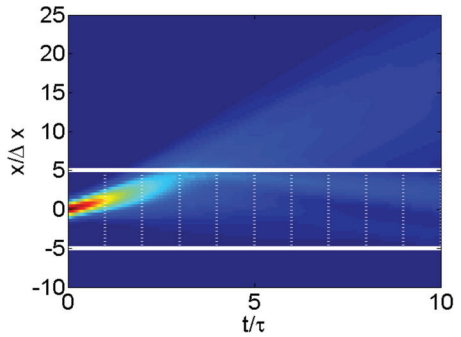


FIG. 2. (Color online) Wave-packet probability exhibits localization in the probe region due to coherent TIE premeasurements. Hot (cold) colors indicate high (low) probability. White horizontal solid lines indicate the probe region and white vertical dotted lines indicate measurement times. Parameters: $w/\Delta_x = 10$, $\Delta_x k_0 = 1$, $\tau/\tau_\infty = 0.5$. Also, $u(x < 0) = \sigma((x + w/2)/(5w))$ and $u(x \geqslant 0) = \sigma((x - w/2)/(5w))$, where $\sigma(x) = 1/(1 + e^{-x})$.

continuous static. Examining the probability distributions $\rho_+(t,x)$ in Fig. 2 reveals that the particle "rebounds" from the probe region boundaries, yet some probability "leaks" out during the intermonitoring interval $\tau$. This leakage, which makes localization incomplete, decreases with the intervals $\tau$.

Localization increases with the rate $1/\tau$, as shown in Fig. 3. Several intriguing conclusions arise from these results: (1) Not only do PMs lead to increased localization as their interval decreases, but the shorter their interval the more enhanced is their localization effect compared to SMs. (2) Impulsive interactions cause stronger localization effects for both SMs and PMs at any rate $1/\tau$, as compared to continuous interactions.

(b) *Exclusion* (Fig. 4). We may exclude the wave packet by repeated SMs or PMs from a chosen probe region if we start performing them prior to the wave-packet arrival. Namely, they can counter the rise in the probability that the wave packet enters the chosen region. In the SM procedure the wave packet's portion inside the region is eliminated by the collapse to the unmeasured state $|0\rangle$, as we monitor "no-click" events [Fig. 6(a)]. In the PM procedure, the interactions also deflect the wave packet from the measured region. Yet here

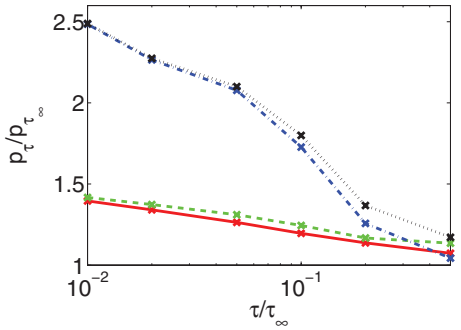


FIG. 3. (Color online) Detection probability as a function of the interaction interval $\tau$ at $t \to \infty$ for static SM (red, solid), impulsive SM (green, dash), static PM (blue, dash-dot) and impulsive PM (black, dotted) interactions. $p_{\tau_\infty}$ is the detection probability of a nonmonitored wave packet at $t \to \infty$. The parameters are the same as in Fig. 2.

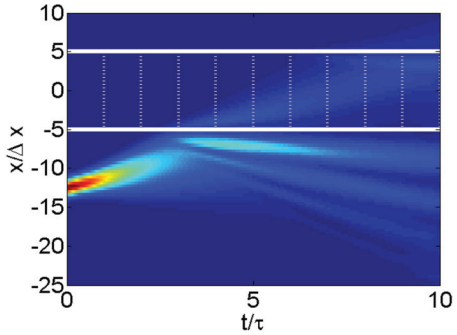


FIG. 4. (Color online) As in Fig. 1, but the wave packet exhibits exclusion from the probe region due to the PM.

the wave-function portion that does penetrate into the region is actually localized or locked by further PMs [Figs. 4 and 6(d), arrow]. Hence, SMs are much more effective as an exclusion scheme than PMs (Fig. 5) for all $\tau$. As in the case of localization, impulsive interactions have a stronger effect than static (continuous) ones, for both SMs and PMs.

The effects of a measurement sequence on free-particle propagation depend on the onset of the sequence, i.e., the time of the first measurement, and the intermeasurement interval. Figure 7 shows that whether the particle is excluded or localized within the probed region crucially depends on these two parameters. The dependence is nontrivial in the sense that (i) the timing of the sequence onset determines whether the outcome will be exclusion or localization; (ii) increasing of the intermeasurement interval changes localization into exclusion and further increase changes it back to localization. The parameter phase space can thus be partitioned into exclusion and localization parts. The timing onset and its intricate interplay with the intermonitoring interval essentially differ from previously considered dynamics, whether by static detection or by repeated measurements [7–9,11–17].

## IV. ANALYSIS

### A. Wave-packet localization without decoherence

Coupling a wave packet to a localized probe via its degenerate (internal) states creates [as per Eq. (3)] translational-internal entanglement [20,21] between the $\psi_0(\boldsymbol{x})$ and $\psi_1(\boldsymbol{x})$ parts of the wave packet and the corresponding probe states $|0\rangle$ and $|1\rangle$. Thereafter, two "tagged" wave packets are formed.

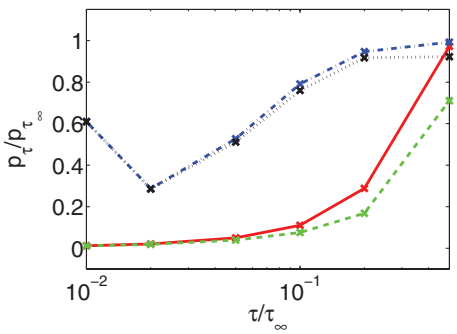


FIG. 5. (Color online) Detection probability as a function of interaction interval $\tau$ at $t \to \infty$ (the same as Fig. 3).

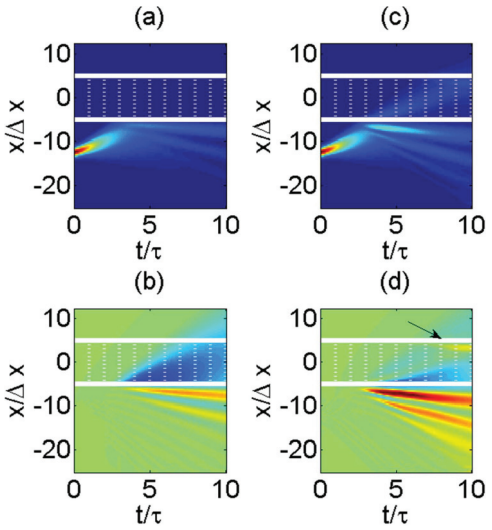


FIG. 6. (Color online) Wave-packet probability exhibits exclusion from the probe region due to (a),(b) selective and (c),(d) premeasurements. Hot (cold) colors indicate high (low) probability. White horizontal solid lines indicate the probe region and white vertical dotted lines indicate measurement times. (a),(c) Wave-packet probability. (b),(d) Wave-packet probability difference from that of the unperturbed propagation.

Each propagates coherently, but they are incoherent with each other: only the incoherent sum of $\rho_+ \equiv \rho_{00} + \rho_{11} = |\psi_0(\boldsymbol{x},t)|^2 + |\psi_1(\boldsymbol{x},t)|^2$ is observed upon tracing out (ignoring) the internal states, which is the source of the PM effects (Fig. 2). Although SMs, which keep track of only one of these wave packets, $\rho_{00}$ or $\rho_{11}$, are expected to have stronger effects on propagation than PMs, this is generally not the case.

Interactions that are effected by transitions between the degenerate (orthogonal) states $|0\rangle$ and $|1\rangle$ change neither the mean energy and momentum of the particle, nor its mean position. By contrast, the dispersion or spread grows under frequent interactions, which redistribute the position probability

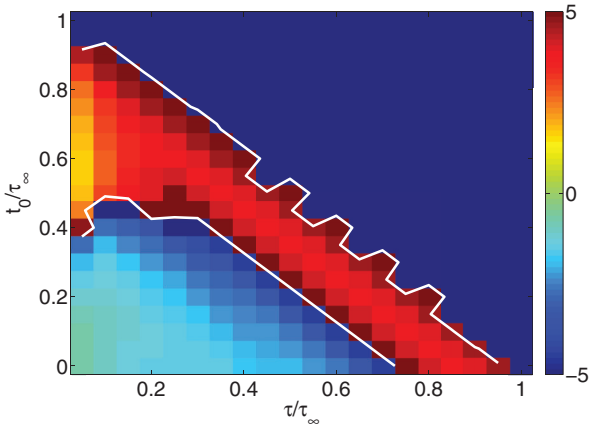


FIG. 7. (Color online) Detection probability as a function of intermeasurement interval $\tau$ and measurement onset $t_0$. The color codes for $\chi = \mathrm{sgn}(1 - p/p_\infty)|\ln(p/p_\infty - 1)|$ are for clarification purposes. Cold (hot) colors denote lower (higher) detection probabilities, meaning exclusion (localization). White lines delineate the boundaries between localization and exclusion.

without affecting its mean. Fully coherent (unitary) $n$-fold TIE interactions ($R = 0$) yield correlated PMs through repeated interferences within each of the wave packets $\psi_0^{(n)}(\boldsymbol{x},t)$ and $\psi_1^{(n)}(\boldsymbol{x},t)$. At the appropriate rate of interventions, the wave packet can be strongly confined within the probe region by interference, while outside that region undetected tails develop and propagate at a speed determined by the probing rate.

Conversely, in order to deflect a particle or ban it from a specific region in space, one can exploit the fact that a detector that does not click provides as much information as one that does, as indicated by the concept of interaction-free measurements [23,24]. Hence, by performing localized frequent SMs or PMs we can reinforce the particle's absence from this region, thus effectively repelling it (Fig. 4).

The repeated interaction between states $|0\rangle$ or $|1\rangle$ (with no decoherence, i.e., $R = 0$) is described by the exact integro-differential equation for either of the wave packets in Eq. (3):

$$\begin{aligned} i\dot{\psi}_{0(1)}(t,\boldsymbol{x}) = &-\frac{\hbar}{2m}\Delta\psi_{0(1)}(t,\boldsymbol{x}) \\ &- gf(t)u(\boldsymbol{x})\int_{-\infty}^{\infty} d\boldsymbol{x}' G(t,\boldsymbol{x}-\boldsymbol{x}')\psi_{1(0)}(0,\boldsymbol{x}') \\ &- g^2 f(t)\int_0^t dt' f(t')\int_{-\infty}^{\infty} d\boldsymbol{x}' u(\boldsymbol{x})u(\boldsymbol{x}') \\ &\times G(t-t',\boldsymbol{x}-\boldsymbol{x}')\psi_{0(1)}(t',\boldsymbol{x}'). \end{aligned} \tag{4}$$

Here $G(t-t',\boldsymbol{x}-\boldsymbol{x}') = [\frac{m}{2\pi i\hbar(t-t')}]^{D/2}\exp[-\frac{m(\mathbf{x}-\mathbf{x}')^2}{2i\hbar(t-t')}]$ is the $D$-dimensional free-particle Green's function. The dynamics is symmetric for $\psi_0(t,\boldsymbol{x})$ and $\psi_1(t,\boldsymbol{x})$ except for the initial wave packet, which is hitherto assumed to be described solely by $\psi_0(0,\boldsymbol{x})$, whereas $\psi_1(0,\boldsymbol{x}) = 0$.

### B. Wave-packet dynamics under decoherence

We next present an extended formalism, where we introduce dephasing of the detector that can result, for example, from a coupling to a dephasing bath or noise. The dephasing rate may be time dependent and is given by $R(t)$. The resulting Lindblad equation is given by (we shall henceforth take $\hbar = 1$)

$$\dot{\tilde{\boldsymbol{\rho}}} = -i[H(t,x),\tilde{\boldsymbol{\rho}}] - \frac{R(t)}{8}[I_S\otimes\sigma_z,[I_S\otimes\sigma_z,\tilde{\boldsymbol{\rho}}]], \tag{5}$$

$$\tilde{\boldsymbol{\rho}} = \boldsymbol{\rho}_{00}|0\rangle\langle 0| + \boldsymbol{\rho}_{01}|0\rangle\langle 1| + \boldsymbol{\rho}_{10}|1\rangle\langle 0| + \boldsymbol{\rho}_{11}|1\rangle\langle 1|, \tag{6}$$

where $\boldsymbol{\rho}_{ij}$ is the particle's density matrix and $\sigma_z = |1\rangle\langle 1| - |0\rangle\langle 0|$.

The resulting Bloch equations are thus given by

$$\dot{\boldsymbol{\rho}}_{00} = \frac{i}{2m}[\Delta,\boldsymbol{\rho}_{00}] - i[\boldsymbol{V}(t,x)\boldsymbol{\rho}_{10} - \boldsymbol{\rho}_{01}\boldsymbol{V}(t,x)], \tag{7}$$

$$\dot{\boldsymbol{\rho}}_{11} = \frac{i}{2m}[\Delta,\boldsymbol{\rho}_{11}] - i[\boldsymbol{V}(t,x)\boldsymbol{\rho}_{01} - \boldsymbol{\rho}_{10}\boldsymbol{V}(t,x)], \tag{8}$$

$$\dot{\boldsymbol{\rho}}_{01} = \frac{i}{2m}[\Delta,\boldsymbol{\rho}_{01}] - i[\boldsymbol{V}(t,x)\boldsymbol{\rho}_{11} - \boldsymbol{\rho}_{00}\boldsymbol{V}(t,x)] - R(t)\boldsymbol{\rho}_{01}/2, \tag{9}$$

$$\dot{\boldsymbol{\rho}}_{10} = \frac{i}{2m}[\Delta,\boldsymbol{\rho}_{10}] - i[\boldsymbol{V}(t,x)\boldsymbol{\rho}_{00} - \boldsymbol{\rho}_{11}\boldsymbol{V}(t,x)] - R(t)\boldsymbol{\rho}_{10}/2 \tag{10}$$

with initial conditions $\boldsymbol{\rho}_{01}(0) = \boldsymbol{\rho}_{10}(0) = \boldsymbol{\rho}_{11}(0) = \mathbf{0}$. Since we are interested only in the measured particle, we define $\boldsymbol{\rho}_+ = \boldsymbol{\rho}_{11} + \boldsymbol{\rho}_{00}$ and $\boldsymbol{\rho}_r = \boldsymbol{\rho}_{01} + \boldsymbol{\rho}_{10}$ and get the two following coupled equations:

$$\dot{\boldsymbol{\rho}}_+ = \frac{i}{2m}[\Delta,\boldsymbol{\rho}_+] - i[\boldsymbol{V}(t,x),\boldsymbol{\rho}_r], \tag{11}$$

$$\dot{\boldsymbol{\rho}}_r = \frac{i}{2m}[\Delta,\boldsymbol{\rho}_r] - i[\boldsymbol{V}(t,x),\boldsymbol{\rho}_+] - R(t)\boldsymbol{\rho}_r. \tag{12}$$

To analytically solve these equations, we turn to the following density matrix representation:

$$\boldsymbol{\rho}_{+,r}(t,\boldsymbol{x}) = \iint d\boldsymbol{x}\rho_{+,r}(t,\boldsymbol{x})|x_1\rangle\langle x_2|, \tag{13}$$

where $\boldsymbol{x} = \{x_1,x_2\}$, $d\boldsymbol{x} = dx_1dx_2$, and $\rho_{+,r}(t,\boldsymbol{x})$ is a function.

Formally integrating Eq. (12) results in

$$\begin{aligned} \rho_r(t,\boldsymbol{x}) = -i\int_0^t dt'\iint d\boldsymbol{x}' e^{-\int_{t'}^t d\tau R(\tau)}\delta V(t',\boldsymbol{x}') \\ \times G(t-t',\boldsymbol{x}-\boldsymbol{x}')\rho_+(t',\boldsymbol{x}'), \end{aligned} \tag{14}$$

$$G(t,\boldsymbol{x}-\boldsymbol{x}') = G(t,x_1-x_3)G^*(t,x_2-x_4), \tag{15}$$

$$\delta V(t,\boldsymbol{x}') = V(t,x_3) - V(t,x_4), \tag{16}$$

where $\boldsymbol{x}' = \{x_3,x_4\}$ and $G(t,x)$ is the Green's function of a free particle. Inserting Eq. (14) into Eq. (11) results in the *exact* integro-differential equation

$$\begin{aligned} \dot{\rho}_+(t,\boldsymbol{x}) = &\frac{i}{2m}\left(\Delta_{x_1} - \Delta_{x_2}\right)\rho_+(t,\boldsymbol{x}) \\ &- \int_0^t dt'\iint d\boldsymbol{x}' e^{-\int_{t'}^t d\tau R(\tau)}\delta V(t,\boldsymbol{x})\delta V(t',\boldsymbol{x}') \\ &\times G(t-t',\boldsymbol{x}-\boldsymbol{x}')\rho_+(t',\boldsymbol{x}'). \end{aligned} \tag{17}$$

This is the probability-density equation, equivalent to Eq. (4), with the important addition of the $e^{-\int_{t'}^t d\tau R(\tau)}$ term.

### C. Analysis results

One can view Eq. (4) [and its proper-dephasing extension Eq. (17)] as a description of a freely propagating particle [the first term on the right-hand side (RHS)] interfering with an initial "source" (the second term on the RHS) and "sources" emanating from previous system-probe interactions (the third term on the RHS). Several time scales determine the interplay between the effects of interactions and the free (unperturbed) evolution of a wave packet of width $\Delta_x$ and mean momentum $p_0 = \hbar k_0$: (i) the particle's group-velocity propagation time scale $t_p = m\Delta_x/\hbar k_0$; (ii) its (unperturbed) dispersion time scale $t_{\rm disp} = m\Delta_x^2/\hbar$; (iii) the measurement interval $\tau$; and (iv) the dephasing (decoherence) interval duration $t_r = 1/R$. We investigate two distinct temporal limits in what follows.

In the impulsive limit, the particle propagates freely between interactions, the instants at which it couples to the probe. In this limit, $T \ll \tau \ll t_p, t_{\rm disp}$, the free-propagating portion $\psi_{0(1)}(\boldsymbol{x},t)$ periodically interferes at $t = n\tau$ with the interactions-induced source, which has the following form, obtained from Eq. (4):

$$\delta\psi_{0(1)}(\boldsymbol{x},n\tau)|_{\rm imp} \cong \frac{\delta(t-n\tau)}{4/\pi^2}\sum_{m=1}^{n-1}\phi_{0(1)}(t,m\tau,\boldsymbol{x}), \tag{18}$$

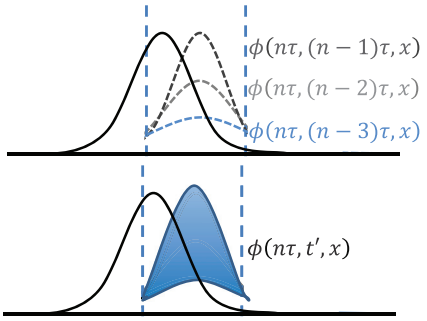


FIG. 8. (Color online) Schematic diagrams of the freely propagating part (solid) and the sources in Eq. (18) (upper diagram) and Eq. (20) (lower diagram).

$$\phi_{0(1)}(t,t',\boldsymbol{x}) = u(\boldsymbol{x}) \int d\boldsymbol{x}' u(\boldsymbol{x}') G(\boldsymbol{x}-\boldsymbol{x}',t-t')\psi_{0(1)}(\boldsymbol{x}',t'), \tag{19}$$

where we used the impulsive full-transfer condition and set $gf(t) \cong (\pi/2)\sum_{n=1}^{N}\delta(t-n\tau)$. The repeated "bursts" of the spatiotemporal nonlocal sources $\sum_{m=1}^{n-1}\phi_{0(1)}(t,m\tau,\boldsymbol{x})$ can give rise to drastic interference with the freely propagating part: each interaction renews the interference, while the previous ones slowly diminish due to their temporal propagation (Fig. 8, upper diagram).

By contrast, in the static limit $\tau \gg t_p, t_{\rm disp}$, the particle continuously interacts with the probe. The source then has the following form:

$$\delta\psi_{0(1)}(\boldsymbol{x},t=n\tau)|_{\rm stat} \cong (\pi^2/4)(1/\tau^2)\int_0^t dt'\phi_{0(1)}(t,t',\boldsymbol{x}), \tag{20}$$

where we used the static full-transfer condition and set $gf(t) = (\pi/2\tau)$. Comparing Eqs. (18) and (20) reveals the reason for the weaker localization effect of the static limit (Fig. 3): the temporal-source interference is suppressed by the low probing rate $1/\tau$ (Fig. 5, lower diagram).

The interaction-induced source crucially depends on the spatial width $w$ of the probe profile $u(\boldsymbol{x})$ relative to the particle wave-packet width at the time of interactions, which we denote by $\Delta_{0(1)}^{(n)}$. In the narrow-probe limit $w \ll \Delta_{0(1)}^{(n)}$, we find that $\phi_{0(1)}(t,t',\boldsymbol{x}) \cong G(\boldsymbol{x}-\boldsymbol{x}_p,t-t')\psi_{0(1)}(\boldsymbol{x}_p,t')$, where $\boldsymbol{x}_p$ is the probe location. Clearly, such a pointlike source cannot strongly affect the spatial distribution or propagation of $\psi_{0(1)}^{(n)}(\boldsymbol{x},t)$. In the broad-probe limit $w \gg \Delta_{0(1)}^{(n)}$, we have $\phi_{0(1)}(t,t',\boldsymbol{x}) \cong u(\boldsymbol{x}_p)\int d\boldsymbol{x}' G(\boldsymbol{x}-\boldsymbol{x}',t-t')\psi_{0(1)}(\boldsymbol{x}',t')$, i.e., the source does not reflect the probe's spatial profile and therefore cannot induce localization. Hence, to maximize the localization (or exclusion) we must enhance the bulk of the wave packet and suppress the tails. Therefore, it is preferable to choose $\Delta_{0(1)}^{(n)} \geqslant w$. In this intermediate case, there is greatly different interference inside and outside the probe region, so that the bulk and the tails are differently affected. In this case the shape of $u(\boldsymbol{x})$ affects the localization: if $u(\boldsymbol{x})$ has abrupt edges, i.e., it is bounded by step functions $\Theta(\boldsymbol{x})$ at $\boldsymbol{x} = \pm\boldsymbol{x}_p$, the generated source in Eq. (18) develops long-range tails [25,26]. In 1D geometry, $\delta\psi_{0(1)}^{(n)}(\boldsymbol{x} > \boldsymbol{x}_p) \propto |\boldsymbol{x}-\boldsymbol{x}_p|^{-3/2}$. Such long tails weaken the localization. A smooth profile of $u(\boldsymbol{x})$ is usually preferable.

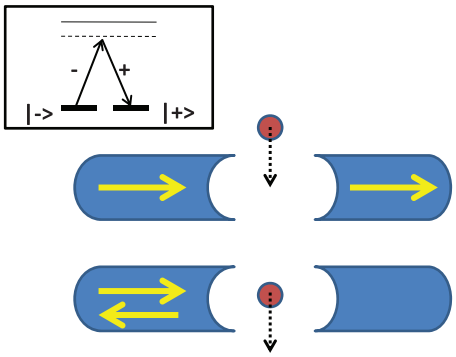


FIG. 9. (Color online) Main panel: PM interactions via photons (yellow arrows) reflected (lower) or transmitted (upper) by a cavity where an atom is present or not, respectively. Inset: PM interaction via stimulated Raman adiabatic passage (STIRAP) transitions between $|-\rangle$ and $|+\rangle$ internal states.

The effects of decoherence (proper dephasing) at rate $R$ between the probe's internal states cannot be incorporated into Eq. (4). Under decoherence, the integro-differential equation for $\rho_+(t,\boldsymbol{x}) = \rho_{00}(t,\boldsymbol{x}) + \rho_{11}(t,\boldsymbol{x})$, has two parts, similarly to Eq. (4), a freely propagating part and a source part. However, this source is diminished by the factor $e^{-R(t-t')}$, which suppresses the temporal effect of previous interaction-induced sources. Since these are essential for the interference effects required for localization, a short decoherence interval $t_R \ll \tau$ results in weaker localization.

## V. DISCUSSION

The present analysis may serve to put Schrödinger's conjecture [1] on firm ground, i.e., infer the fundamental limitations on localization by observation: the spatial width of the wave packet should be broader (but not by much) than the probe, and the observation should not be "continuous," i.e., static, but rather consist of impulsive acts, well separated within the dispersion or group-velocity time. This crucial dependence of localization on PM intervals and their timing is basically different from Zeno-like evolution [7–19]. The present approach demonstrates localization and exclusion solely from phase interference and translational-internal entanglement considerations, and not from energy-momentum transfer as in previous approaches [2–6,27]. Remarkably, the mere tagging of wave-packet parts by correlating them to orthogonal discrete states leads to PM effects of same-state consecutive interferences that may cause either localization or exclusion of the wave packet. Several feasible experimental scenarios are given below.

*Probing atoms by a cavity*. One such experiment consists of an atom falling through a cavity [28,29] while Raman-resonant light impinges on the cavity at different onset times and intensity or rate (Fig. 9). The atom's exclusion from the cavity occurs if the PM starts prior to the atom's entrance. Localization (suspension) within the cavity occurs if the PM starts when the atom is inside. If the states are nearly degenerate, there is no momentum transfer to the atom during

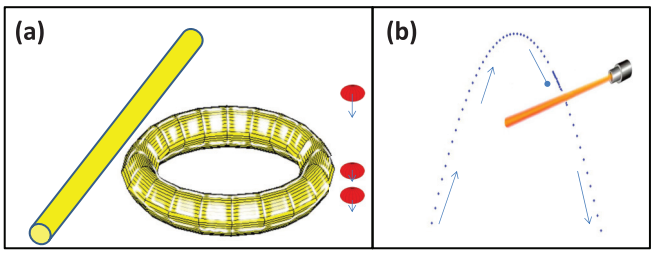


FIG. 10. (Color online) Experimental scenarios. (a) Microresonator (toroid), wherein photon interaction with the falling cold atoms (spheres) can localize the atoms near the resonator (arrow lengths indicate speed) and increase their interaction duration. (b) Atomic fountain setup with a localization or exclusion laser in its descending path, which induces internal Raman transitions at a rate $1/\tau$. The density of the dots indicates speed.

the Raman excitation and the pulse temporal shaping is a control parameter.

*Probing atoms by microresonators*. Another feasible experimental scenario for SMs may involve falling atoms that interact with light fields inside a microresonator [29], Fig. 10(a). The detection of the photons exiting the resonator to a coupled waveguide indicates the presence of an atom near it. The photons probe the presence of an atomic wave packet near the resonator, the states $|0\rangle$ and $|1\rangle$ corresponding to a transmitted and reflected photon, respectively. In a typical experimental setup [29], 10 $\mu$K atoms with $\Delta_x = 50$ nm fall from a height of at least 1 mm that leads to velocity $v = 0.1$ ms$^{-1}$. A photon detection interval of $\tau = 100$ ns then suffices to achieve the atom localization effects described above. The atom's exclusion from the cavity occurs if the SM starts prior to the atom's entrance, where localization (suspension) occurs if the SM starts when the atom is inside the cavity.

*Probing an atomic fountain*. A feasible experimental scenario for PMs may involve an atomic fountain, which is crossed on its way down by a tightly (wavelength-scale) focused laser beam. The laser radiation consists of two copropagating beams that cause a Raman transition between two hyperfine or magnetic ground-state sublevels of the atom, $|0\rangle|-\rangle$ and $|1\rangle|+\rangle$, Fig. 10(b). For localization of the wave packet (and, hence, delay in its fall) to take place, the first Raman interaction should occur when the cloud enters the laser region, while for deflection the Raman pulses should occur prior to the cloud's arrival. By varying the timing and the interpulse intervals, the effects described above may be demonstrated. A PM repetition period $\tau = 100$ ns is realistic, if we consider a stimulated Raman process (STIRAP) [30] with the peak Rabi frequency $\sim 2\pi \times 5$ MHz (i.e., with the intensity $\sim 2$ mW/cm$^2$).

These setups emphasize the unique character of the proposed localization scheme, by enabling a PM without (or with negligible) energy-momentum exchange, via Raman transition between near-degenerate states. We conclude that the predicted effects may lead to additional probe-induced trapping or steering procedures for quantum light and matter.

## ACKNOWLEDGMENTS

We acknowledge the support of DIP, ISF, and FWF (Project No. Z118-N16).

[1] E. Schrödinger, *Mind and Matter* (The University Press, Cambridge, 1959).
[2] C. M. Caves and G. J. Milburn, Phys. Rev. A **36**, 5543 (1987).
[3] J. I. Cirac, A. Schenzle, and P. Zoller, Europhys. Lett. **27**, 123 (1994).
[4] J. B. Mackrory, K. Jacobs, and D. A. Steck, New J. Phys. **12**, 113023 (2010).
[5] Y. Japha and G. Kurizki, Phys. Rev. Lett. **77**, 2909 (1996).
[6] Y. Japha, V. M. Akulin, and G. Kurizki, Phys. Rev. Lett. **80**, 3739 (1998).
[7] A. Konetchnyi, M. Mensky, and V. Namiot, Phys. Lett. A **177**, 283 (1993).
[8] P. Facchi and S. Pascazio, J. Phys. A **41**, 493001 (2008).
[9] M. B. Mensky and S. Stenholm, Phys. Lett. A **308**, 243 (2003).
[10] A. M. Lane, Phys. Lett. A **99**, 359 (1983).
[11] A. G. Kofman and G. Kurizki, Nature (London) **405**, 546 (2000).
[12] P. Facchi and S. Pascazio, Prog. Opt. **42**, 147 (2001).
[13] A. G. Kofman and G. Kurizki, Phys. Rev. Lett. **87**, 270405 (2001).
[14] M. C. Fischer, B. Gutierrez-Medina, and M. G. Raizen, Phys. Rev. Lett. **87**, 040402 (2001).
[15] A. G. Kofman and G. Kurizki, Phys. Rev. Lett. **93**, 130406 (2004).
[16] P. Facchi, D. A. Lidar, and S. Pascazio, Phys. Rev. A **69**, 032314 (2004).
[17] P. Facchi, S. Pascazio, A. Scardicchio, and L. S. Schulman, Phys. Rev. A. **65**, 012108 (2001).
[18] G. J. Milburn, J. Opt. Soc. Am. B **5**, 1317 (1988).
[19] W. M. Itano, D. J. Heinzen, J. J. Bollinger, and D. J. Wineland, Phys. Rev. A **41**, 2295 (1990).
[20] N. Bar-Gill and G. Kurizki, Phys. Rev. Lett. **97**, 230402 (2006).
[21] M. Kolar, T. Opatrny, N. Bar-Gill, N. Erez, and G. Kurizki, New J. Phys. **9**, 129 (2007).
[22] G. Gordon, Europhys. Lett. **83**, 30009 (2008).
[23] A. C. Elitzur and L. Vaidman, Found. Phys. **23**, 987 (1993).
[24] P. Kwiat, H. Weinfurter, T. Herzog, A. Zeilinger, and M. A. Kasevich, Phys. Rev. Lett. **74**, 4763 (1995).
[25] I. Bialynicki-Birula and Z. Bialynicka-Birula, Phys. Rev. A **79**, 032112 (2009).
[26] G. Kurizki, A. Kozhekin, and A. Kofman, Europhys. Lett. **42**, 499 (1998).
[27] R. B. Diener, B. Wu, M. G. Raizen, and Q. Niu, Phys. Rev. Lett. **89**, 070401 (2002).
[28] J. Volz, R. Gehr, G. Dubois, J. Esteve, and J. Reichel, Nature (London) **475**, 210 (2011).
[29] B. Dayan, A. S. Parkins, T. Aoki, E. P. Ostby, K. J. Vahala, and H. J. Kimble, Science **319**, 1062 (2008).
[30] H. Theuer, R. G. Unanyan, C. Habscheid, K. Klein, and K. Bergmann, Opt. Express **4**, 77 (1999).